Microstructural characterization and fatigue response of alloy Ti-46Al-5Nb-1W with varied surface quality and thermal exposure history

Huang, Zheng; Lin, J. P.; Feng, B.

DOI:
10.1016/j.matchar.2017.06.004

Document Version
Peer reviewed version

Citation for published version (Harvard):
Huang, Z, Lin, JP & Feng, B 2017, 'Microstructural characterization and fatigue response of alloy Ti-46Al-5Nb-1W with varied surface quality and thermal exposure history', *Materials Characterization*, vol. 130, pp. 285-297. https://doi.org/10.1016/j.matchar.2017.06.004

Accepted Manuscript

Microstructural characterization and fatigue response of alloy Ti-46Al-5Nb-1W with varied surface quality and thermal exposure history

Z.W. Huang, J.P. Lin, B. Feng

PII: S1044-5803(16)30394-1
DOI: doi: 10.1016/j.matchar.2017.06.004
Reference: MTL 8704

To appear in: *Materials Characterization*

Received date: 27 September 2016
Revised date: 17 May 2017
Accepted date: 1 June 2017

Please cite this article as: Z.W. Huang, J.P. Lin, B. Feng , Microstructural characterization and fatigue response of alloy Ti-46Al-5Nb-1W with varied surface quality and thermal exposure history, *Materials Characterization* (2017), doi: 10.1016/j.matchar.2017.06.004

Microstructural characterization and fatigue response of alloy Ti-46Al-5Nb-1W with varied surface quality and thermal exposure history

Z.W. Huang[a,b*] J.P. Lin[c] and B. Feng[a]

a School of Materials Science and Engineering, Southwest Jiaotong University, Chengdu, Sichuan, 610031, P.R. China

b School of Metallurgy and Materials, The University of Birmingham, Edgbaston, Birmingham B15 2TT, U.K.

c State Key Laboratory for Advanced Metals and Materials, University of Science and Technology Beijing, Beijing 100083, China

∗Corresponding author, Tel: +44 121 4143436

Email address: z.w.huang@bham.ac.uk

The stress controlled fatigue behaviour of a coarse-grained fully lamellar TiAl alloy Ti-46Al-5Nb-1W has been investigated under no exposure, block exposure and individual exposure-oxidation conditions (exposure for 10000 h at 700°C) to assess the effects of surface roughness, stress concentration, oxidation and inner microstructural changes. The alloy is observed to be sensitive to surface damage, but less sensitive to V-notch even after exposure because the surface area sampling the highest stress significantly reduces the EDM impact and exposure effect. Unlike grain-refined alloys, both shot peening and electropolishing offered a moderate and roughly the same increase in fatigue limit, indicating that for a coarse-grain fully lamellar alloy the control factor for fatigue is lamellar colony size. Fatigue performances are improved for all surfaces when subjected to block exposure, attributed to a long-term annealing which outweighs the harmful effects from microstructural embrittlement. After individual exposure-oxidation, fatigue performance deteriorates significantly for the shot peened and moderately for the electropolished but not for the EDM wired. The behaviour can be understood based on whether or not the beneficial changes outweigh the detrimental changes for a specific surface.

Microstructural characterization and fatigue response of alloy Ti-46Al-5Nb-1W with varied surface and thermal exposure history

The stress controlled fatigue behaviour of a coarse-grained fully lamellar TiAl alloy Ti-46Al-5Nb-1W has been investigated under no exposure, block exposure and individual exposure-oxidation conditions (exposure for 10000 h at 700°C) to assess the effects of surface roughness, stress concentration, oxidation and inner microstructural changes. The alloy is observed to be sensitive to surface damage, but less sensitive to V-notch even after exposure because the surface area sampling the highest stress significantly reduces the EDM impact and exposure effect. Unlike grain-refined alloys, both shot peening and electropolishing offered a moderate and roughly the same increase in fatigue limit, indicating that for a coarse-grain fully lamellar alloy the control factor for fatigue is lamellar colony size. Fatigue performances are improved for all surfaces when subjected to block exposure, attributed to a long-term annealing which outweighs the harmful effects from microstructural embrittlement. After individual exposure-oxidation, fatigue performance deteriorates significantly for the shot peened and moderately for the electropolished but not for the EDM wired. The behaviour can be understood based on whether or not the beneficial changes outweigh the detrimental changes for a specific surface.

Key words: Titanium aluminides; Electron microscopy; Fatigue behavior; Oxidation; Phase transformation; Thermal stability;

1. Introduction

Unlike Ti-based and Ni-based alloys, TiAl-based alloys often show steep fatigue crack growth resistance curves. Combined with their modest fracture toughness, such behavior reveals the problem of defining a safe life for the intermetallic alloys [1-4]. One solution is to use conventional S-N fatigue curves to determine total life [5, 6]. However, uncertainty may still arise since steep crack growth resistance curves usually give rise to relatively “flat” S-N curves [7-9]. In such circumstances, it is necessary to predict the level of in-service stresses accurately and to find the ways that can enhance S-N performance.

In reality, surface defects and other stress concentration raisers, resulting from component design, machining, foreign object damage and surface oxidation, significantly change the total life of γ–TiAl components. The impacts should be determined quantitatively. Previous studies have been done to assess the effects of surface quality [10-13], notches [14, 15], foreign object damage [16, 17] and oxidised layers [18, 19] on the fatigue properties of TiAl alloys. However, much less work has been done for the TiAl alloys which undergo a long-term thermal exposure. A γ-TiAl alloy component of an aero-engine is in fact exposed to elevated temperatures in air for long term. Three major types of changes are expected to occur: a) inner microstructual changes owing to dissolution and phase transformation, b) surface oxidation and c) changesof stress profile in the interior and at the surfaces of the componenet. For the sake of safty, it is imperative to assess the influences of all these changes on fatigue life under the condition of long-term thermal exposure in air.

This study describes some efforts made in assessment of all these effects on the total

life of an intermediate-strength, coarse-grained fully lamellar γ-TiAl alloy. The main objective is to reveal how and to what extent the varied stress concentration and surface/bulk material changes affect the fatigue performance of the TiAl alloy which is subjected to a 10000-h exposure at 700°C in air.

2. Experimental

Coarse grain full lamellar alloy with a nominal composition of Ti-46Al-5Nb-1W (at.%, named alloy 46Al-5Nb-1W) was cast into a Φ100 mm ingot using a double-melted PACH (Plasma Arc Cold Hearth) process. The ingot was hot isostatically pressed (HIPped) at 1260°C/150 MPa for 4 hours, followed by a stabilisation heat treatment at 900°C for 24 hours.

Three groups of specimens were prepared for S-N fatigue testing: Group A, no exposure; Group B, exposed in ingot block (without oxidation); Group C, exposed in individual specimen (with surface oxidation). Bend specimens of dimensions 70 mm x 10 mm x 10 mm were cut using electro-discharge machining (EDM). Four types of surfaces were prepared for each group: 1) plane-sided wire EDM, 2) V-notched wire EDM, 3) shot-peened and 4) electropolished. The details of the preparation procedures were listed in Table 1. Following surface preparation, specimens in Group A were fatigue tested directly (designated "no exposure"), while specimens in Group C were exposed individually in an air-circulated furnace at 700°C for 10000 h ("individual exposure-oxidation"), and then tested after exposure. In contrast to Group C, Group B was exposed as a Φ100 mm ingot block ("block exposure") in the same furnace at 700°C for 10000 h, and then machined to shape and prepared for the same four surfaces, followed by fatigue testing. It appears that all specimens in Group B exhibited interior microstructural changes but no oxidation on the surface.

Table 1 Preparation procedure of the maximum stressed surface for fatigue tests

Four types of surface studied	Preparation procedure
EDM, plain-sited	EDM, 1 pass to shape
V notch (Kt = 3)	EDM, 1 pass to shape
Shot peening	EDM, 1 pass, grinding, shot peening
Electropolishing	EDM, 1 pass, grinding and polishing, electropolishing

A 60° V-shaped notch with a root radius of 0.20 mm and overall notch depth of 1.75 mm was introduced, which resulted in an elastic stress concentration factor $K_t = 3$. Notch was machined using one pass EDM, same as plane-sided EDM specimens. It should be noted that the notch was introduced after block exposure for Group B but before individual exposure-oxidation for Group C. For Group A, it was introduced and tested directly. For shot peening samples, a 150-200 μm thick layer was removed by mechanical grinding to diminish the influence EDM-damaged surface before peening. Shot peening was performed by means of an injector type system using spherical zirconia-based ceramic shot with an average diameter range of 0.4-0.5 mm The air-jet pressure used was 5×10^5 Pa. The peening was done to achieve a full coverage of the maximum-stressed surface. Electropolishing was conducted on mechanically ground-polished samples and performed at 20 volts in an electrolytic solution (6% perchloric acid, 35% butanol and 59% methanol) at - 30°C.

Surface conditions were quantified by surface roughness traces (Ra values) measured by an Ambios XP-2 profilometer. All Ra values are given in Table 2. The surface roughness of Group A and B under the same surface condition is similar. Therefore, their surface roughness values are listed together for the two non-oxidised groups. On the other hand, the surface roughness of Group C was measured after individual exposure-oxidation for 10000 h at 700°C. As seen in Table 2, compared with Group A and B, the long-term individual exposure-oxidation caused a marginal increase in roughness for EDM surface and a more considerable increase for the shot peened and a significant increase for the electropolished.

Microhardness of shot peened surface was measured with a HXD-1000TM Vickers microhardness tester, using a load of 500 g. The distance of the indentation marks was greater than five indentations apart. The results presented are the average of the three-five measurements per position. The average standard deviation of the hardness values was 20 HV0.5 in Group A and B and 14 HV0.5 in Group C.

Table 2 Surface roughness Ra (μm) with error range for each surface and exposure condition.

Specimen (Group)	EDM (A, B)	Shot peening (A, B)	Electropolishing (A, B)	EDM (C)	Shot peening (C)	Electropolishing (C)
Surface roughness Ra (μm)	4.65±0.1	1.53±0.2	0.26±0.04	5.15±0.28	2.16±0.06	1.06±0.11

The stress controlled S-N fatigue tests were conducted at room temperature using a PLG-100 electromagnetic resonance testing machine at a frequency of ~100 Hz under a stress ratio R of 0.1. Four point bending samples (70 mm x 10 mm x10 mm) were loaded with a maximum stressed span of 20 mm and a distance of 20 mm between the inner and outer rollers. Each sample was cycled until either failure or run-out, which was defined as 10^7 cycles. The fatigue limit σ_{FL} is typically defined by the value of σ_{max} at run-out.

The various surfaces and inner microstructures were characterised for all the three thermal exposure conditions using scanning electron microscopy (SEM) and transmission electron microscopy (TEM). Image analysis was carried out to quantify varied microstructural constituents using Image J software on SEM BSE (back scattered electron) images. TEM specimens were prepared by twin-jet polishing with an electrolyte of 5 vol. % perchloric acid, 30 vol. % butan-1-ol and 65 vol. % methanol, operating at 30 V and at a temperature of -30°C. TEM was performed using a JEOL 2010 FX microscope operating at 200 kV. The measurement of α_2 lamellae thickness was done by tilting the foils such that the lamellar interfaces were edge-on (i.e. orientated along $<1\bar{1}0>_\gamma$ // $<11\bar{2}0>_{\alpha 2}$ directions). A linear-intercept method using AxioVision software was utilised to quantify such parameters. For all quantitative results, mean values were determined with a standard deviation to represent the uncertainty of the measurements.

3. Results

3.1 The microstructure before exposure

Fig. 1a and 1b shows the BSE microstructure of alloy 46Al-5Nb-1W before exposure. The structure after HIPping and stabilisation was almost a full lamellar (FL) and consisted of colonies (94 vol. %) of α_2 (lighter lath) and γ (darker lath) lamellae, plus small amounts of equiaxed γ and β (the lightest phase) around colony boundaries. The volume fraction and

mean size (with the error range) of all the microstructural constituents determined by image analysis are listed in Table 3 for the ally before and after thermal exposure. The mean size of lamellar colonies was measured to be 635 μm (± 211 μm), and about 15% lamellar colonies were larger than 900 μm in size. The α_2 lamellae are relatively fine in thickness, which is 70.6±33.5 nm from TEM.

Table 3 Volume fraction (VF) and size of microstructural constituents in alloy 46Al-5Nb-1W before and after thermal exposure.

Exposure time (h)	Size of lamellar colony (μm)	VF of α_2 lamellae in lamellar colonies (%)	Thickness of α_2 lamellae (nm)	VF of β grains (%)	VF of γ grains (%)
0	635±211	13.5±2.5	70.6±33.5	1.8±0.3	4.3±2.2
10000	692±216	3.1±1.2	59.9±47.8	2.0±0.7	4.1±1.6

About 2 vol. % primary β was retained due to coring effects during solidification of the highly alloyed TiAl alloy containing β stabilisers W and Nb [20]. Fig. 2a, a bright field (BF) image, shows a β grain with a matt surface. Corresponding diffraction patterns in Fig. 2b reveals that the retained β has a B2 structure and contains ω phase. The ω phase has already reached a mature, fully crystalline condition after HIPping but shows a shape effect. As observed in Fig. 2b, the maxima from ω show short streaks perpendicular to $[\bar{2}22]_\beta$ and $[2\bar{2}2]_\beta$ directions in the $[110]_\beta$ pattern. This is consistent with the suggestion that the initial ω phase embedded in the bcc B2 matrix has a rather two-dimensional morphology which is very thin and about a few nanometers in diameter, lying on $\{222\}_\beta$ planes [21, 22].

3.2. The microstructure after exposure

After exposure for 10000 h at 700°C, inside microstructure changed extensively in alloy 46Al-5Nb-1W. The changes are characterised by three typical decomposition processes.

The first occurred on α_2 lamellae. Relatively fine α_2 lamellae were rarely decomposed in parallel orientation. They thinned gradually instead (Fig. 1c), and some of the fine α_2 lamellae decomposed longitudinally along the lamellar length, resulting in phase transformation of γ sections from individual α_2 laths ($\alpha_2 \rightarrow \gamma$).

The second type of decomposition, which also occurred on α_2 lamellae, was found to be a universal phenomenon throughout lamellar colonies. As shown in the Fig. 1d, widespread formation of numerous fine particles was observed universally on α_2 lamellae. These particles are acicular in shape and show specific orientation to the parent α_2 laths. TEM investigation conducted previously has confirmed that they are β(B2+ω) particles [23]. The results indicate clearly that the long-term exposure at 700°C has induced a phase transformation of $\alpha_2 \rightarrow$ β(B2+ω), resulting in the dissolution of α_2 lamellae. Such a phase transformation was reported previously for varied W-containing TiAl alloys [24-26]. Quantitative TEM investigation revealed that the volume fraction of α_2 lamellae decreased from 13.5% to 3.1% after 10000 h exposure at 700°C [27].

The third change occurred in prior β (B2+ω) grains. Very fine ω precipitates present before exposure grew to sub-micron sized ω blocks after 10000 h exposure. TEM centered dark field (CDF) image in Fig. 2c reveals that the grown ω are crowded inside the original β

block, leaving some spaces unoccupied. Corresponding diffraction patterns from the block confirms the co-existence of the coarsened ω and remnant β matrix (Fig. 2d). Also observed in the diffraction patterns is disappearance of the two-dimensionality of original ω thin disks. The growing process of ω is associated with the diffusion of W from ω into the β matrix, whereas Nb diffuses from the β matrix into ω. As revealed by the atomic number contrast in BSE images (Fig. 1d and the insert in Fig. 2c), the remnant β shows network morphology, brighter in colour than ω particles. The composition change during ω growth from the β/B2 matrix was already reported in [28, 29]. The present suggests that a well-developed ω grain would reach a near-equilibrium composition which is enriched in Nb, while the remaining β/B2 matrix would be further stablised by W enrichment.

3.3. The fatigue-specimen surfaces prepared before exposure and after block exposure

The four types of surface in Group B after block exposure are very similar in morphology and chraracter to their counterparts in Group A, respectively. This is because the surfaces were always prepared after specimen-cutting from Φ100 ingot block. They are therefore not described independently here. The following description holdsfor both groups.

The surface damage caused by one-pass wire EDM consisted of widespread holes, protruded globes and fine cracks (Fig. 3a). The Ra value is high (Ra=4.65 μm) as shown in Table 2. The induced cracks were penetrated at a depth of ~ 50 μm beneath the surface (Fig. 3b). A high level of tensile residual stress (289 MPa) was detected by authors on a similar processed one-pass EDM wired surface using the "blind hole" drilling technique [7]. It is deduced that the residual tensile stress on the present EDM wired surface should be similar to this level.

The structural changes induced by shot peening are demonstrated in Fig. 4. Normal view in Fig. 4a reveals shallow dimples, puckers and short cracks. The Ra value was decreased to 1/3 of the EDM value, Ra=1.53 μm. There is a clearly deformed zone underneath the peened surface, as shown by cross-sectional view of the peened specimen in Fig. 4b, which extends over a length scale of ~ 40 μm. It should be mentioned that the same peening process produced a deformation zone of 15-25 μm in depth for its grain-refined version: alloy 44Al-5Nb-1W-1B, reflecting the different yield stresses of the two materials [30]. Considerable bending and kinking of the α_2 and γ lamellae occurs as demonstrated in Fig. 4b and 4c. It was generally suggested that α_2 lamellae may only be deformed elastically owing to higher solution hardening since α_2 in α_2+γ two-phase alloys scavenges interstitial impurities like oxygen, carbon and nitrogen [31, 32]. Dynamic recrystallization and phase transformation occurred inside the deformed surface layer, which can be observed only on γ laths. As arrowed in Fig. 4c, the conversion of microstructure due to deformation is characterised by dissolution of the α_2 lamellae and nucleation of small equiaxed γ grains in the γ lamellae (indicated by fine arrows). Mechanical twining is also observable in the γ lamellae (indicated by coarse arrow).

Owing to the process-induced deformation, the microhardness in the near-surface regions increased considerably, with a maximum value at the surface. Both the specimens without exposure (Group A) and the specimens with block exposure (Group B) show a ~ 300 μm-thick hardened region where the surface is 105 HV0.5 harder than the bulk material,

increased by 36% (Fig. 5). It is noted that Group A and B show almost the same hardened layer because the only difference between them was the inner microstructural changes occurred in the latter.

For Group C samples, however, shot peening was conducted before individual exposure. As shown in Fig. 5, the individually exposed-oxidised samples demonstrate a significantly reduced near-surface hardening region. The enhanced hardness value by peening was decreased from 400 MPa before exposure to 325 MPa after it, only 10% higher than the bulk value. The thickness of the hardened region reduced to 150 μm, which is half the originally hardened depth, attributed to stress relaxation by exposure and oxidation. Thermal relaxation of surface hardening is a widely observed phenomenon. As reported previously, both the microhardness and compressive residual stress induced by shot peening can be reduced significantly after 50-h annealing at 650°C [13]. A stress relief mechanism was suggested, which may result from relatively easy annealing-out of unstable debris defects [13] and from defect rearrangement, which has been recognised by HRTEM (high-resolution transmission electron microscopy) observation [33]. Normal view of the elecropolished surface before exposure is presented in Fig. 6a. Roughness of the elecropolished surface was decreased significantly, Ra=0.26 μm, which is less than 1/5 of the shot-peened value. It is realised that all the procedures used (mechanical grinding, polishing and final electropolishing) are capable of removing a ~150-200 μm thick surface layer, which can get rid of the whole EDM-damaged surface layer. The surface defects were therefore eliminated sufficiently. Observation from a cross sectional view in Fig. 6b reveals that such a surface finish on the maximum-stress side is smooth and nearly defect-free.

3.4. The fatigue-specimen surfaces after individual exposure and oxidation

Individual exposure and oxidation of samples in Group C resulted in bulk material changes and surface oxidation. Fig. 7a, the normal view of the EDM specimens, demonstrates that the impaired surface remains coarse and uneven. Surface roughness trace Ra is barely changed (4.65 μm to 5.15 μm). Cross sectional examination reveals that the scale is about 10-15 μm thick, arrowed in Fig. 7b. High density of oxidised pits formed in the subsurface layer, about 50 μm below the surface. It seems that oxygen diffused through the EDM-induced surface cracks, inducing subsurface oxidation. More importantly, microstructural changes were observed just below the loose layer, below which numerous small particles with strong atomic number contrast formed at the expense of α_2 lamellae, producing an α_2-free layer with 5 μm width, as arrowed in Fig. 7c. They were assumed to be Nb-W enriched oxides. During oxidation, main elements Ti, Al, Nb, W were expected to release with gradual dissolution of α_2. While Ti and Al were used to form TiO_2-Al_2O_3 oxides at outer surface, W and Nb were accumulated under the loose layer to form such white particles.

Compared to EDM samples, the normal view of the thin scale on shot peened surface looks relatively integrated, although shallow dimples are still observable (Fig. 8a). Oxidation has worsened the surface roughness by ~40%, from 1.53 μm to 2.16 μm. Cross sectional examination reveals that the oxide scale is about 5 μm thick, thinner than its EDM counterpart (Fig. 8b). The α_2 lamellae dissolution under the loose surface is less severe for the shot peened than for the EDM wired. However, numerous white particles are observed to

spread across ~ 10 μm distance from the surface. These particles are normally short needle-shaped (Fig. 8c). They are assumed to be the W-/Nb-containing oxides. The real identity remains unknown. It is not very clear why the oxides/precipitates cover a wider distance, although a higher quality of surface and less dissolution of α_2 lamellae occurred on the shot peened surface.

For the elecropolished surface, the loose scale formed after 10000 h exposure-oxidation is hardly observable. However, the thin scale revealed lamellar morphology (Fig. 9a) because different oxides formed above the γ-TiAl lamellae and α_2-Ti_3Al lamellae. As examined by reference [34] using EDX analysis, the oxides on γ-TiAl lamellae consisted of an Al-rich oxide, likely Al_2O_3; while the oxides on α_2-Ti_3Al lamellae consisted of an Al-rich oxide covered by a very porous and discontinuous Ti-rich oxide, probably rutile TiO_2. Accordingly, the surface roughness Ra increased from 0.26 μm to 1.06 μm. Cross sectional view in Fig. 9b and 9c has found that a semi-continuous layer consisting of white particles formed under the loose scale. The narrow semi-continuous layer, roughly 1 μm thick and covered both α_2 and γ lamellae, was also observed on the same electropolished surface after the same individual exposure-oxidation for 44Al-5Nb-1W-1B. EDX analysis of the white layer conducted previously revealed that the layer is enriched in W, Nb and Ti, and contains a small amount of oxygen [30]. It indicates that the heavier metals W, Nb and Ti which originally partitioned in α_2 lamellae would be released from α_2 dissolution and diffused towards the surface, accumulating to form a white layer below the thin loose scale. Below the semi-continuous layer, only a few white oxide particles observed inside the surface. This is very different from that found in shot peened surface layer, indicating that the electropolished surface is more resistant to oxygen attack than the shot peened surface, although the latter has a compressive-stress layer.

3.5. The stress-controlled fatigue behavior before exposure (Group A)

Stress-controlled fatigue curves of the four surfaces are demonstrated in Fig. 10a-c for the three groups. The fatigue curves of the each exposure groups are compared in Fig. 11a-d for four types of surface. For multiple run-outs, a lower value was used for defining the fatigue limit. The values of the fatigue limit (fatigue strength) obtained are shown and analysed in Table 4 for three plane-sited surfaces (EDM, shot peening and electropolishing) and in Table 5 for the V-notched. The ratio of $\sigma_{FL}/\sigma_{0.2}$ is also included. All the percentage data in the two tables are approximated to the nearest integer.

The fatigue limit is only 235 MPa for EDM plane-sided surface before exposure, giving the ratios of $\sigma_{FL}/\sigma_{0.2}$=0.50 and σ_{FL}/σ_{UTS}=0.46. The remarkably low ratios appear to be related to EDM surface which contains prevalent surface defects and a high level of tensile residual stresses. It is of interest to note that the ratios are almost the same as those ($\sigma_{FL}/\sigma_{0.2}$=0.52 and σ_{FL}/σ_{UTS}=0.48) obtained by grain-refined high strength alloy 44Al-5Nb-1W-1B ($\sigma_{0.2}$=568 MPa) [30]; but significantly lower than those obtained by another intermediate strength alloy Ti-45Al-2Mn-2Nb-0.8vol%TiB_2($\sigma_{0.2}$= 486 MPa), where the same EDM surface provided a ratio $\sigma_{FL}/\sigma_{0.2}$ = 0.78 and σ_{FL}/σ_{UTS} = 0.73 [34]. This seems to suggest that the degree of sensitivity to surface damage is not always reversely related to alloy yield strength.

Table 4 Fatigue results and data analysis for EDM, shot peening and electropolishing specimens, $\sigma_{0.2}$= 470 MPa, 398 MPa and 290 MPa in Group A, B and C, respectively.

Exposure Group	Surface condition	σ_{FL} (MPa)	$\sigma_{FL}/\sigma_{0.2}$	Change in σ_{FL}(%) relative to EDM	Change in σ_{FL}(%) relative to Group A	Change in σ_{FL}(%) relative to Group B
	EDM	235	0.50	—	—	—
A	Shot peening	280	0.60	19	—	—
	Electropolishing	290	0.62	23	—	—
	EDM	310	0.78	—	32	—
B	Shot peening	320	0.80	3	14	—
	Electropolishing	380	0.95	23	31	—
	EDM	300	1.03	—	28	-3
C	Shot peening	180	0.62	-40	-36	-44
	Electropolishing	250	0.86	-17	-14	-34

The increase in the fatigue limit (σ_{FL}) after shot peening is relatively moderate, raised by 19%. The moderate improvement to 280MPa is agreement with the moderate hardening obtained on the peened surface. As depicted in section 3.3, although an outer layer of 300 μm in depth was hardened by the bombarded streams, only 36% hardening was produced. However, the same peening process raised the σ_{FL} by 80% for alloy 4522-0.8, a grain refined lamellar alloy. It clearly points out that the coarse grained alloy 46Al-5Nb-1W is less able to be improved by shot peening.

The enhancement of the fatigue strength after electropolishing is also non-significant, raised by 23% from 235 MPa to 290 MPa. The improvement is similar to that achieved by shot peening. The similarity in improvement by shot peening and by electropolishing over EDM is considered to be related to the coarse FL colonies of the alloy. Also noticed is that the 23% increase in σ_{FL} is similar to 26% increase obtained by alloy 4522-0.8 where the same electropolishing procedure was employed [34]. All the moderate improvements are tentatively attributed to a loading condition of $\sigma_{max} > \sigma_{0.2}$ for the two intermediate strength alloys, for which activation of plastic deformation on the maximum-stressed surfaces is relatively easy to occur.

The S-N fatigue results of the V notched (Kt=3) samples are listed in Table 5. It is found that the σ_{FL} reduced considerably in all the three exposure conditions, but not to the extent that the Kt (theoretical elastic stress concentration factor) would have predicted. A fatigue notch factor $K_f = 1.36$ and a ratio of $K_f/K_t = 0.45$ is gained for non-exposed condition. K_f, notch factor, represents the effectiveness of the notch in decreasing $\sigma_{FL,}$ obtained based on σ_p/σ_n (σ_p and σ_n are the fatigue limit for plane-sided and notched specimens, respectively). If K_f is close to the value of K_t, the material is thought to be sensitive to notch. The ratio of $K_f/K_t = 0.45$ in Group A, which is well below the maximum value $K_f/K_t = 1$, indicates a low notch sensitivity for the non-exposed alloy 46Al-5Nb-1W. The notch sensitivity is also represented by notch sensitivity factor Q ($Q = K_f\text{-}1/K_t\text{-}1$). As seen in Table 5, Q is 0.18 for Group A, which is also significantly far from the extreme value 1.

The long term thermal exposure did not increase or decrease the notch sensitivity significantly. The notch sensitivity factor Q for the exposed specimens with and without surface oxidation still remains far from the extreme value of 1, as listed in Table 5.

Table.5 S-N fatigue results and data analysis for V notch (K_t=3) specimens

Group	σ_{FL}(MPa)	$\sigma_{FL}/\sigma_{0.2}$	K_f	K_f/K_t	Notch sensitivity factor Q	Increase in σ_{FL}(%) relative to Group A
A	173	0.37	1.36	0.45	0.18	—
B	185	0.46	1.68	0.56	0.34	5
C	200	0.69	1.50	0.50	0.25	16

3.6. The stress-controlled fatigue behavior after block exposure (Group B)

Comparison between Fig. 10a and 10b has revealed that all the four surfaces in Group B achieve better fatigue performance than its counterpart in Group A. The improvement is detailed in Table 4 and 5. A significant increase (32%) was obtained on EDM surface, a mild but observable increase (14%) on the shot peened and a significant increase (31%) on the electropolished. However, the σ_{FL} remains almost unchanged after block exposure for the V-notched.

The enhanced fatigue behaviour is believed to originate from an annealing-like effect. Soaking of the ingot block in a warm-air (700°C) environment for 10000 h is believed to relax and dissipate the stress concentration caused by ingot casting and by phase transformations such as $\alpha_2 \rightarrow \beta$ [35] and $\beta \rightarrow \omega$ [36] to some degree. The defects and segregates could be inactivated and alleviated partially by such a long-term warm soaking. These are sure to be beneficial to fatigue resistance, even on an already damaged EDM surface. However, one must remember that a detrimental effect from microstructural changes is also introduced by block exposure, which includes 1) decomposition of α_2 lamellae into fine γ laths and sections, 2) universal decomposition of α_2 lamellae to fine β (B2+ω) particles and 3) precipitation and growth of ω particles from β(B2) grains to form ω blocks (section 3.2). As detailed in previous study, decomposition of α_2 lamellae and formation of ω blocks indicated an "oxygen-releasing embrittlement" and "ω formation embrittlement" to the alloy [30], together reducing fatigue strength.

The present results indicate clearly that the beneficial effect of annealing outweighs the detrimental effect from microstructure embrittlement for all the four types of surface. This observation is different from that observed on fine grain alloy 44Al-5Nb-1W-1B, on which the same block exposure reduced fatigue performance for both the peened and electropolished except for the EDM wired which remains essentially unchanged [30]. The reason for the different reaction can be explained by considering the difference in α_2 volume fraction and morphology between the two alloys. The α_2 lamellae are 30% less in volume fraction and 60% thinner in thickness in the Al-rich, B-free alloy than in Al-lean, B containing alloy 44Al-5Nb-1W-1B [23]. Accordingly, the "oxygen-releasing embrittlement" and the "ω formation embrittlement" are less in degree and extent. Therefore, the fatigue properties of the 5Nb-1W alloy are less compromised.

3.7. The stress-controlled fatigue behavior after individual exposure-oxidation (Group C)

As seen in Fig. 10c and Table 4, shot peening and electropolishing make the fatigue strength inferior to its counterpart in Group A after individual exposure-oxidation: a significant decrease (-36%) for the shot peened and a mild decrease (-14%) for the electropolished. This reveals that the harmful effect of oxidation, plus detrimental effect from

microstructural embrittlement, finally outweighs the beneficial effect from long-term annealing.

The shot peened resulted in a severely deteriorated fatigue limit (180 MPa) after individual exposure-oxidation, compared with 280MPa before exposure and 320 MPa after exposure without oxidation. This was caused by the harmful effects both from oxidation and from partially disappearance of compressive stress/hardened surface. With the fast recovery of surface hardening, the surface is only 10% harder than the bulk material after individual exposure-oxidation, while it was 36% harder than bulk alloy in Group A and B. These, associated with negative effect of microstructural embrittlement, are expected to outweigh the positive effect of long-term annealing significantly, therefore reducing the fatigue strength significantly.

The electropolished surface shows moderately deteriorated fatigue strength after the individual exposure-oxidation. The fatigue limit was reduced to 250 MPa, compared with 290MPa before exposure and 380 MPa in block exposure without oxidation. The harm done by oxidation appears to be less severe on a nearly defect-free surface than on a hardened/compressively-stressed surface when subjected to a long-term thermal exposure. It is reasonable to assume that the surface roughness is a key factor against oxidation at 700°C. With a much reduced surface roughness (Ra=0.26 μm) produced by electropolishing, the ability against oxidation is well above that produced by shot peening (Ra=1.53 μm).

In contrast to the two improved surfaces, as listed in Table 4 and 5, the plane-sided EDM shows 28% increase and the V-notched EDM shows 16% increase in σ_{FL} over non-exposed condition. It seems to indicate that the formation of a thicker oxidised layer is not harmful enough to bring down σ_{FL} for the two EDM wired surfaces. Even more unexpected is that the EDM plain-sited surface produced a highest σ_{FL} among the four surfaces, which is 300 MPa, significantly higher than those produced either by shot peeing (180 MPa) or by electropolishing (250 MPa). The higher fatigue limit for the two EDM wired surfaces is difficult to be rationalised. Although the residual tensile stresses were relaxed and the surface stress raisers could become less activated, the crack initiation resistance which is higher than those on two improved surfaces is still out of expectation. More work needs to be done to double check it.

4. **Discussion**

4.1. Controlling mechanism in the coarse lamellar alloy

After surveying three grain-refined alloys, a reverse relationship between damage sensitivity and yield strength is found for the EDM surface. As listed in Table 6, a higher yield strength alloy produces a lower fatigue limit σ_{FL}, and a lower $\sigma_{FL}/\sigma_{0.2}$, σ_{FL}/σ_{UTS} ratio, indicating that the fatigue performance of high strength alloys is highly sensitive to the EDM damage. With reduced yield strength, the fatigue behaviour can become less sensitive to the damaged surfaces.

Table 6 Changes in $\sigma_{FL}/\sigma_{0.2\,(0.1)}$ and σ_{FL}/σ_{UTS} ratios with varied strength for lamellar-based γ-TiAl alloys, obtained for one pass EDM wired surface before exposure

Alloy	Colony	$\sigma_{0.2(0.1)}$	σ_{UTS}	σ_{FL}	$\sigma_{FL}/\sigma_{0.2(0.1)}$	σ_{FL}/σ_{UTS}

	size (μm)	(MPa)	(MPa)	(MPa)		
Ti-44Al-4Nb-4Zr-0.2Si-1B [37]	71±11	620	665	280	0.45	0.42
Ti-44Al-5Nb-1W-1B [30]	115±46	568	605	293	0.52	0.48
Ti-45Al-2Mn-2Nb-0.8vol.TiB_2[34]	82±34	486	524	380	0.78	0.73
Ti-46Al-5Nb-1W	635 ± 211	470	507	235	0.50	0.46

It appears that the reverse relationship only applies to grain-refined alloys. As seen in Table 6, the average colony size is less than 120 μm for the first three alloys. For alloy 46Al-5Nb-1W, however, the average lamellar colony size is 635 ± 211 μm. Very high damage sensitivity ($\sigma_{FL}/\sigma_{0.2}$ = 0.50 and σ_{FL}/σ_{UTS} = 0.46 for EDM surfaces) is observed for the alloy. The present results point out clearly that the surface damage could be more harmful to a coarse grained alloy. As suggested by other researchers, there exist difficulties in defining a critically initiated crack sizes in lamellar alloys in fatigue [6, 8, 38, 39]. This is particularly true for a coarse-grained lamellar alloy because coarse lamellar colonies provide a higher degree of uncertainty to fatigue resistance. Short sized defects are easier to become a dominantly initiated crack along lamellar interfaces when initiated cracks stay in an extra-large colony and in a soft orientation.

4.2 Effect of surface quality on fatigue strength

It is well known that both electropolishing and shot peening are sure to promote fatigue crack initiation resistance. However, based on our previous research on three grain-refined FL/NL alloys, which surface is more effective in improving fatigue behaviour over the EDM wired actually depends on alloy strength (Table 7). The surface prepared by electropolishing outperforms the surface prepared by shot peening for high strength alloys: 44Al-5Nb-1W-1B (73% vs. 50%) and 44Al-4Nb-4Zr-0.2Si-1B (68% vs. 36%). This is elucidated by the fact that the high yield strength alloys are less able to absorb the impact of shot stream by plastic deformation than low/intermediate strength alloys. A less deep deformation and a less intense compressive-stress zone is introduced to the surface layer. As shown in Fig. 12a, a shallow deformation layer (~20 μm deep) was produced by shot peening for alloy 44Al-5Nb-1W-1B. However, the high strength alloy provides a loading condition of $\sigma_{max} < \sigma_y$ for majority of the fatigue specimens [30, 37]. Plastic deformation resulted from dislocation slipping/twining is difficult to form in surface layer. Without intense deformation, the designed surface with or without stress raisers becomes increasingly important for fatigue crack initiation. Therefore, the defect-free surfaces from electropolishing would certainly show a higher fatigue crack nucleation/initiation resistance since a crack nucleation stage is needed before critical initiation.

Table.7 Increase in fatigue limit (σ_{FL}) by shot peening and electropolishing, relative to EDM surface in four lamellar-based γ-TiAl alloys before exposure. (Group A)

Alloy	$\sigma_{0.2/0.1}$ (MPa)	Surface condition	σ_{FL} (MPa)	increase in σ_{FL}(%) relative to EDM
		EDM	293	—
Ti-44Al-5Nb-1W-1B [30]	568	Shot peening	440	50
		Electropolishing	507	73
Ti-44Al-4Nb-4Zr-0.2Si-1B [37]	621	EDM	280	—

			380	36
			470	68
			380	36
		Shot peening	380	36
			470	68
			470	68
		Electropolishing	380	36
			470	68
			380	—
		EDM	550	45
			480	26
Ti-45Al-2Mn-2Nb-0.8 vol%TiB_2 [34]	486	Shot peening	550	45
			480	
		Electropolishing		26
		EDM	235	—
Ti-46Al-5Nb-1W	470	Shot peening	280	19
		Electropolishing	290	23

The reverse is true for the intermediate strength alloy of Ti-45Al-2Mn-2Nb-0.8 vol%TiB_2. The shot peened surface is more capable of increasing σ_{FL} than the electropolished (45% vs 26%). The reason is simply related to the effectiveness of shot peening. Alloy with relatively lower yield strength (486 MPa) is better able to absorb the impact of shot particles by plastic deformation than high yield strength alloys. A deeper penetrating plastic deformation zone is introduced to the surface layer, bringing an increased resistance to crack initiation. This is shown in Fig. 12b, the same shot peening process produced a deformation layer of ~80 μm in depth for alloy 4522-0.8. On the other hand, for the moderately strengthened alloy a loading condition of $\sigma_{max} > \sigma_y$ often applies for the electropolished specimens [34], where planar slipping and twining are likely to activate at maximum-stressed surfaces. Microcracks are therefore relatively easy to nucleate, even on a "defect-free" surface, resulting in a reduced degree of fatigue crack initiation resistance.

For the present alloy 46Al-5Nb-1W with intermediate yield strength $\sigma_{0.2}$ = 470 MPa, the fatigue behaviour observed is quite different from aforementioned three alloys. As seen in Table 7, both shot peening and electropolishing of the EDM surface after mechanical grinding offered a roughly same increase: 19% by peeing and 23% by electropolishing. More importantly, the degree to which the fatigue performance is improved by the two methods is relatively low. The results tend to indicate again that for a coarse-grain FL alloy the control factor in determining fatigue behaviour is lamellar colony size rather than yield strength.

4.3. Controlling mechanism for V notch specimens

The present experiment on V notch specimens has achieved significantly low notch sensitivity for all the three exposure conditions. It is well known that coarse lamellar alloys normally show lower notch sensitivity than grain-refined alloys [7]. To some

degree, the reduced notch sensitivity is related to notch strengthening, which occurs due to localised plastic deformation since stresses concentrated to the notch root. This is true for the intermediate strength alloy since a loading condition of $\sigma_{max} > \sigma_y$ (the σ_{max} at notch root is defined by taking into account of K_t) applied.

However, it would be inappropriate if only considering local plasticity and notch strengthening. As seen in Table 5, very similar fatigue limit and notch sensitivity were obtained for all the three exposure conditions. It is deduced that a sampling effect could be the controlling factor in determining the notch fatigue behaviour rather than any internal and external effects caused. It is well known that only the surface area or the volume ahead of the V notch root is sampled by the highest stresses, causing notch strengthening owing to local plasticity and work hardening. The surface area/volume is significantly smaller in the V-notched than in the plane-sited EDM surface. For the latter, a maximum stressed span of 20 mm with a width of 10 mm is used. It appears that the V-notch significantly reduces the EDM-induced damaging impact. This could be one of the reasons for the quite low notch sensitivity observed here. Also observed is that the exposure effects, either beneficial (annealing) or detrimental (microstructural embrittlement and oxidation) are all restricted to a very limited notch-root region, therefore hardly affecting the notch fatigue behaviour.

4.4. Effect of block exposure on fatigue strength

It is generally recognised that two contradictory effects occur during block exposure of a Φ 100 ingot-cast block. 1) A beneficial effect, coming from long-term warm soaking, acts as annealing to relax and dissipate the stress concentration, and consolidate microstructure. 2) A detrimental effect, caused by decomposition of α_2 lamellae and formation of brittle phases, induces “oxygen-releasing embrittlement” and “ω formation embrittlement” to the alloy.

Table.8 The change in fatigue limit (σ_{FL}) from no exposure (A) to block exposure (B) in four lamellar-based γ-TiAl alloys

Alloy	$\sigma_{0.2/0.1}$ (MPa)	Surface condition	σ_{FL} in A (MPa)	σ_{FL} in B (MPa)	Change in % relative to A
Ti-44Al-5Nb-1W-1B [30]	568	EDM	293	310	6
		Shot peening	440	400	-9
		Electropolishing	507	430	-15
Ti-44Al-4Nb-4Zr-0.2Si-1B [37]	621	EDM	280	240	-14
			380	350	-8
			470	340	-28
		Shot peening	380 380 470	350	-8
		Electropolishing	470 380 470	340	-28
Ti-45Al-2Mn-2Nb-0.8 vol%TiB_2 [34]	486	EDM	380	400	5
			380	350	-8
			470	340	-28

		Shot peening	550 380 470	635	15
		Electropolishing	480 380 470	615	28
		EDM	235	310	32
Ti-46Al-5Nb-1W	470	Shot peening	280	320	14
		Electropolishing	290	380	31

However, both increased and decreased fatigue limits were observed in the block exposed over the no-exposed after surveying four lamellar TiAl alloys. As shown in Table 8, grain-refined high strength alloys Ti-44Al-4Nb-4Zr-0.2Si-1B and Ti-44Al-5Nb-1W-1B show a noticeable decrease, while intermediate strength alloys Ti-45Al-2Mn-2Nb-0.8vol%TiB_2 and Ti-46Al-5Nb-1W show a noticeable increase for all the three surfaces. The reason for this can be found by specifically considering the two contradictory effects for individual alloys. It is reasonable to believe that the beneficial annealing effect owing to stress relaxation and microstructural consolidation should be roughly the same for all the four alloys. Therefore, the different fatigue strength listed in Table 8 is deduced to be affected mainly by variable degree of microstructural embrittlement.

The α_2 lamellae in alloy 46Al-5Nb-1W is 30% less in volume fraction and 60% thinner in thickness than in alloy 44Al-5Nb-1W-1B [23, 27]. The "oxygen-releasing embrittlement" owing to α_2 decomposition and the "ω formation embrittlement" owing to $\alpha_2 \rightarrow \beta(B2+\omega)$ transformation and B2+ω coarsening are deduced to be less in degree and extent. A reduced impact from microstructural embrittlement on fatigue may occur, allowing the beneficial effect to outweigh the detrimental effect. Tensile tests performed at 700°C for the two alloys support this suggestion. A similar circumstance was also found in alloy 4522-0.8, in which no significant dissolution of α_2 lamellae occurred and no B2+ω phase existed [40]. Without the considerable negative impacts, the enhanced fatigue behaviour observed is mainly attributed to the long-term annealing effect.

For alloy Ti-44Al-4Nb-4Zr-0.2Si-1B, on the other hand, prevalent formation of γ grains, $D8_8$-ω particles and silicides occurred during exposure. They are brittle in nature, thereby causing the detrimental effect to outweigh the beneficial effect from annealing. The ductility was therefore reduced from 0.79% to 0.21%, reduced by 73%, for this alloy [41].

In summary, under the same annealing effect, the actual fatigue performance after block exposure is mainly decided by the degree and extent of exposure-induced microstructural embrittlement, which is changeable from alloy to alloy.

4.5 Effect of individual exposure-oxidation on fatigue strength

In consideration of the same exposure applied to all the individual specimens in Group C, both the beneficial and detrimental effects occurred in Group B should also occur in Group C. That is: the warm air annealing-like effect (beneficial) and the exposure-induced embrittlement (detrimental). Besides the two, extra effects were introduced to specific surfaces. The extra effects are variable from surface to surface and discussed in detail as

below.

For EDM wired surfaces, soaking in 700°C air environment for 10000°C leads to an extra detrimental and an extra beneficial effect on fatigue. Surface oxidising is certainly detrimental to fatigue, whereas relaxation and dissipation of tensile residual stresses is beneficial to fatigue. Surveying four FL/NL TiAl alloys conducted so far has found that the worst EDM surfaces are of the highest potential in increasing fatigue performance over shot peening and electropolishing when individually exposed-oxidised. As listed in Table 9, leaving aside what happens to these alloys for the varied degree of enhancement, all these alloys demonstrate highest percentage increase for the EDM surface over the two improved surfaces. This phenomenon states clearly that the relaxation/dissipation of surface tensile stresses, together with the universal benefit from long-term annealing, outweighs the negative effects of exposure-induced embrittlement and surface oxidation.

Table.9 The change in fatigue limit (σ_{FL}) from no exposure (A) to individual exposure-oxidation (C) in four lamellar-based γ-TiAl alloys

Alloy	$\sigma_{0.2/0.1}$ (MPa)	Surface condition	σ_{FL} in A (MPa)	σ_{FL} in C (MPa)	Change in % relative to A
Ti-44Al-5Nb-1W-1B [30]	568	EDM	293	330	13
		Shot peening	440	250	-43
		Electropolishing	507	450	-11
Ti-44Al-4Nb-4Zr-0.2Si-1B [37]	621	EDM	280	450	61
			380	350	-8
			470	340	-28
		Shot peening	380 380 470	475	25
		Electropolishing	470 380 470	530	13
Ti-45Al-2Mn-2Nb-0.8 vol%TiB_2 [34]	486	EDM	380	500	32
			380	350	-8
			470	340	-28
		Shot peening	550 380 470	510	-7
		Electropolishing	480 380 470	570	19
Ti-46Al-5Nb-1W	470	EDM	235	300	28
		Shot peening	280	180	-36
		Electropolishing	290	250	-14

The lowest fatigue strength(σ_{FL} = 180 MPa)was obtained by shot peening surface. The mechanism behind this is suggested by considering extra detrimental effects encountered by the pre-enhanced surface. Besides the two contradictory effects mentioned for Group B, two

extra detrimental effects emerged during individual exposure-oxidation, 1) oxidation damage in surface layer, and 2) the softening of hardened surface and relaxing of compressive stresses. These, together with the negative effect of exposure-induced embrittlement, are expected to outweigh the positive effect of bulk material annealing.

A less severe decrease in σ_{FL} was found on electropolished surface. Following the consideration for beneficial (annealing) and detrimental (microstructural embrittlement) effects, there is only one extra detrimental effect, oxidation, acting on the nearly defect-free surface. Moreover, the negative effect of oxidation becomes less harmful to fatigue when surface roughness did not deteriorate to a scale observed on shot peened surface: 1.06 μm for electropolishing vs 2.16 μm for shot peening. Therefore, the surface roughness rather than the pre-hardened condition is considered to be a controlling factor in retaining fatigue strength. This is true for both grain refined high strength and non-grain refined intermediate strength alloys, as shown in Table 9. It is therefore evident that with 10000 h exposure-oxidation, a defect-free surface rather than a pre-hardened surface is more effective in retaining oxidation resistance in all the four alloys.

5. Conclusions

1. Coarse grained alloy Ti-46Al-5Nb-1W is sensitive to surface damages, showing a ratio $\sigma_{FL}/\sigma_{0.1}$ =0.50 and σ_{FL}/σ_{UTS} =0.46 for EDM surface.
2. The same alloy with EDM surface is much less sensitive to V-notch. The notch sensitivity factor Q is 0.18 before exposure and little changed after exposure. This is attributed to the very small surface area/volume sampling the highest stress, which significantly reduces the EDM damage impact.
3. Unlike grain-refined alloys, both shot peening and electropolishing offered a moderate and roughly the same increase in σ_{FL}. The control factor for fatigue behaviour of a coarse-grain FL alloy is suggested to be lamellar colony size.
4. Fatigue performances are improved for all types of surface when subjected to block exposure, ascribed to a long-term annealing effect which outweighs the harmful effects from microstructural embrittlement.
5. Fatigue performance deteriorated significantly for the shot peened and moderately for the electropolished but not for the EDM wired after individual exposure-oxidation. The fatigue behaviour can be understood individually based on whether or not the beneficial changes outweigh the detrimental changes for a specific surface.
6. Electropolished surface surpasses the shot peened when subjected to 10000-h individual exposure-oxidation for the coarse lamellar alloy, suggesting that a defect-free surface rather than a pre-hardened surface is more competent in retaining oxidation resistance.

Acknowledgement

This work was supported by the National Natural Science Foundation of China (Grant number: 51271154); the State Key Laboratory for Advanced Metals and Materials, University of Science and Technology Beijing (Grant number: 2012-ZD03). The author ZWH is also

very thankful to the School of Metallurgy and Materials, The University of Birmingham, U. K. for some experimental support.

References

[1]. A.W. James, P. Bowen, Elevated temperature crack growth resistance of TiAl under monotonic and cyclic loading, Mater Sci Eng A 153 (1992) 486-492.

[2]. C. Mercer, J. Lou, S.M. Allameh, W.O. Soboyejo, Effects of Temperature on the Fatigue Crack Growth Behavior of Cast Gamma-Based Titanium Aluminides, Metall Mater Trans A 32 (2001) 2781-2794.

[3]. Y. Mutoh, S.J. Zhu, T. Hansson, S. Kurai, Y. Mizuhara, Effect of microstructure on fatigue crack growth in TiAl intermetallics at elevated temperature, Mater Sci Eng A 323 (2002) 62–69.

[4]. J. Yang, H. Li, D. Hu, M. Dixon, Microstructural characterisation of fatigue crack growth fracture surfaces of lamellar Ti45Al2Mn2Nb1B, Intermetallics 45 (2014) 89-95.

[5]. B.D. Worth, S.J. Balsone, J.W. Jones, An overview of the structural capability of available gamma titanium aluminide alloys, in: Y-W. Kim, R. Wagner, M. Yamaguchi (Eds), Gamma Titanium Aluminides, TMS, Warrendale, PA, 1995, pp. 821-834.

[6]. J.M. Larsen, A.H. Rosenberger, B.D. Worth, K. Li, D.C. Maxwell, W.J. Porter, Assuring reliability of gamma titanium aluminides in long-term service, in Kim Y-W, D.M. Dimiduk, M.H. Lorreto (Eds), Gamma Titanium Aluminides, TMS Warrendale, PA, 1999, pp. 463-472.

[7]. S.J. Trail, P. Bowen, Effects of stress concentrations on the fatigue life of a gamma-based titanium aluminide, Mater Sci Eng A 192/193 (1995) 427-434.

[8]. G. Henaff, A-L. Gloanec, Fatigue properties of TiAl alloys, Intermetallics 13 (2005) 543-558.

[9]. S.K. Jha, J.M. Larsen, A.H. Rosenberger, The role of competing mechanisms in the fatigue life variability of a nearly fully-lamellar γ-TiAl based alloy, Acta Mater 53 (2005) 1293–1304.

[10]. P.E. Jones, D. Eylon, Effects of conventional machining on high cycle fatigue behavior of the intermetallic alloy Ti-47Al-2Nb-2Cr (at.%), Mater Sci Eng A 263 (1999) 296–304.

[11]. A.R.C. Sharman, D.K. Aspinwall, R.C. Dewes, P. Bowen, Workpiece surface integrity considerations when finish turning gamma titanium aluminide, Wear 249 (2001) 473–481.

[12]. X. Wu, D. Hu, M. Preuss, P.J. Withers, M.H. Loretto, The role of surface condition, residual stress and microstructure on pre-yield cracking in Ti44Al8Nb1B, Intermetallics 12 (2004) 281–287.

[13]. J. Lindemann, C. Buque, F. Appel, Effect of shot peening on fatigue performance of a lamellar titanium aluminide alloy, Acta Mater 54 (2006) 1155–1164.

[14]. W.E. Voice, M. Henderson, E.F.J. Shelton, X. Wu, Gamma titanium aluminide, TNB, Intermetallics 13 (2005) 959–964.

[15]. M. Nazmy, M. Staubli, G. Onofrio, V. Lupinc, Surface defect tolerance of a cast TiAl alloy in fatigue, Scripta Mater 45 (2001) 787-792.

[16]. T.S. Harding, J.W. Jones, P.S. Steif, T.M. Pollock, Room temperature fatigue response of γ–TiAl to impact damages, Scripta Mater 40 (1999) 445–449.

[17]. M.R. Bache, C.C. Morgans, Domestic object damage and fatigue behaviour of an advanced gamma TiAl alloy, Intermetallics 19 (2011) 782-786.

[18]. S.K. Planck, A.H. Rosenberger, The influence of high temperature exposure on the mechanical performance of a γ titanium aluminide alloy, Mater Sci Eng A 325 (2002) 270–280.

[19]. A. Zeller, F. Dettenwanger, M. Schutze, Influence of water vapour on the oxidation behaviour of titanium aluminides, Intermetallics 10 (2002) 59–72.

[20]. Z.W. Huang, Inhomogeneous microstructure in highly alloyed cast TiAl-based alloys, caused by microsegregation, Scripta Mater 52 (2005) 1021-1025.

[21]. Z.W. Huang, W.E. Voice, P. Bowen, Thermal stability of Ti-46Al-5Nb-1W alloy, Mater Sci Eng A 329-331 (2002) 435-445.

[22]. G. Shao, P. Tsakiropoulos, Prediction of ω phase formation in Ti–Al–X alloys, Mater. Sci. Eng. A 329-331 (2002) 914–919.

[23]. Z.W. Huang, J.P. Lin, H.L. Sun, Microstructural changes and mechanical behaviour of a near lamellar γ-TiAl alloy during long-term exposure at 700°C, Intermetallics 85 (2017) 59-68.

[24]. J.G. Wang, T.G. Nieh, Creep of a beta phase-containing TiAl alloy, Intermetallics 8 (2000) 737–748.

[25]. D.Y. Seo, J. Beddoes, L. Zhao, G.A. Botton, The influence of aging on the microstructure and creep behaviour of a γ-Ti–48%Al–2%W intermetallic, Mater Sci Eng A 329–331 (2002) 810–820.

[26]. M.A. Morris-Munoz, I. Gil, D.G. Morris, Microstructural stability of γ-based TiAl intermetallics containing β phase, Intermetallics 13 (2005) 929-936.

[27]. Z.W. Huang, H.L Sun, Microstructural stability and mechanical behaviour of a coarse-grained fully lamellar alloy Ti-46Al-5Nb-1W, unpublished results, 2017.

[28]. L. Song, X.J. Xu, L. You, Y.F. Liang, J.P. Lin, Phase transformation and decomposition mechanisms of the βo(ω) phase in cast high Nb containing TiAl alloy, J Alloys and Compounds 616 (2014) 483–491.

[29]. M. Schloffer, B. Rashkova, T. Schoberl, E. Schwaighofer, Z. Zhang, H. Clemens, S. Mayer, Evolution of the ω_o phase in a β-stabilized multi-phase TiAl alloy and its effect on hardness, Acta Materialia 64 (2014) 241–252.

[30]. Z.W. Huang, J.P. Lin, Z.X. Zhao, H.L. Sun, Fatigue response of a grain refined TiAl alloy Ti-44Al-5Nb-1W-1B with varied surface quality and thermal exposure history, Intermetallics 85 (2017) 1-14.

[31]. R. Uemori, T. Hanamura, H. Morikawa, Oxygen scanvenging effect of the α_2 phase in the TiAl intermetallic compound, Scripta Metall Mater 26 (1992) 969-974.

[32]. A. Denquin, S. Naka, A. Huguet, A. Menand, Atom-probe investigation of the partitioning of interstitial elements in two-phase $\gamma+\alpha_2$ TiAI-based alloys, Scripta Metall Mater 28 (1993) 1131-1136.

[33]. F. Appel, Atomic level observations of mechanical damage in shot peened TiAl, Phil Mag 93 (2013) 2-21.

[34]. Z.W. Huang, S. Huang, On the role of thermal exposure on the stress controlled fatigue behaviour of an intermediate strength γ-TiAl based alloy. Mater Sci Eng A 636 (2015) 77–90.

[35]. P. Pe´rez, J.A. Jime´nez, G. Frommeyer, P. Adeva, Oxidation behaviour of a Ti–46Al–1Mo–0.2Si alloy: the effect of Mo addition and alloy microstructure, Mater Sci Eng A 284 (2000) 138–147.

[36]. D. Zhang, G. Dehm, H. Clemens, Effect of heat-treatmens and hot-isostatic pressing on phase transformation and microstructure in a β/B2 containing γ-TiAl based alloy, Scripta Mater 42 (2000) 1065–1070.

[37]. Z.W. Huang, C. Sun, On the role of thermal exposure on the stress controlled fatigue behavior of a high strength titanium-aluminum alloy, Mater Sci Eng A 615 (2014) 29-41.

[38]. B.D. Worth, J.M. Larsen, A.H. Rosenberger, Threshold fatigue crack growth behavior of the gamma titanium aluminide alloy Ti-46.5Al-3Nb-2Cr-0.2W under high cycle fatigue conditions, in M.V. Nathal, R. Darolia, C.T. Liu, P.L. Martin, D.B. Miracle, R. Wagner, M. Yamaguchi (Eds), Structural Intermetallics, TMS Warrendale, PA, 1997, pp. 563-569.

[39]. T.S. Harding, J.W. Jones, Evaluation of a threshold-based model of the elevated-temperature fatigue of impact-damaged γ-TiAl, Metall Mater Trans A, 32 (2001) 2975-2984.

[40]. Z.W. Huang, W. Hu, Thermal stability of an intermediate strength fully lamellar Ti-45Al-2Mn-2Nb-0.8vol.% TiB2 alloy, Intermetallics 54 (2014) 49-55.

[41]. Z.W. Huang, Thermal stability of Ti-44Al-4Nb-4Zr-0.2Si-1B alloy, Intermetallics 42 (2013) 170-179.

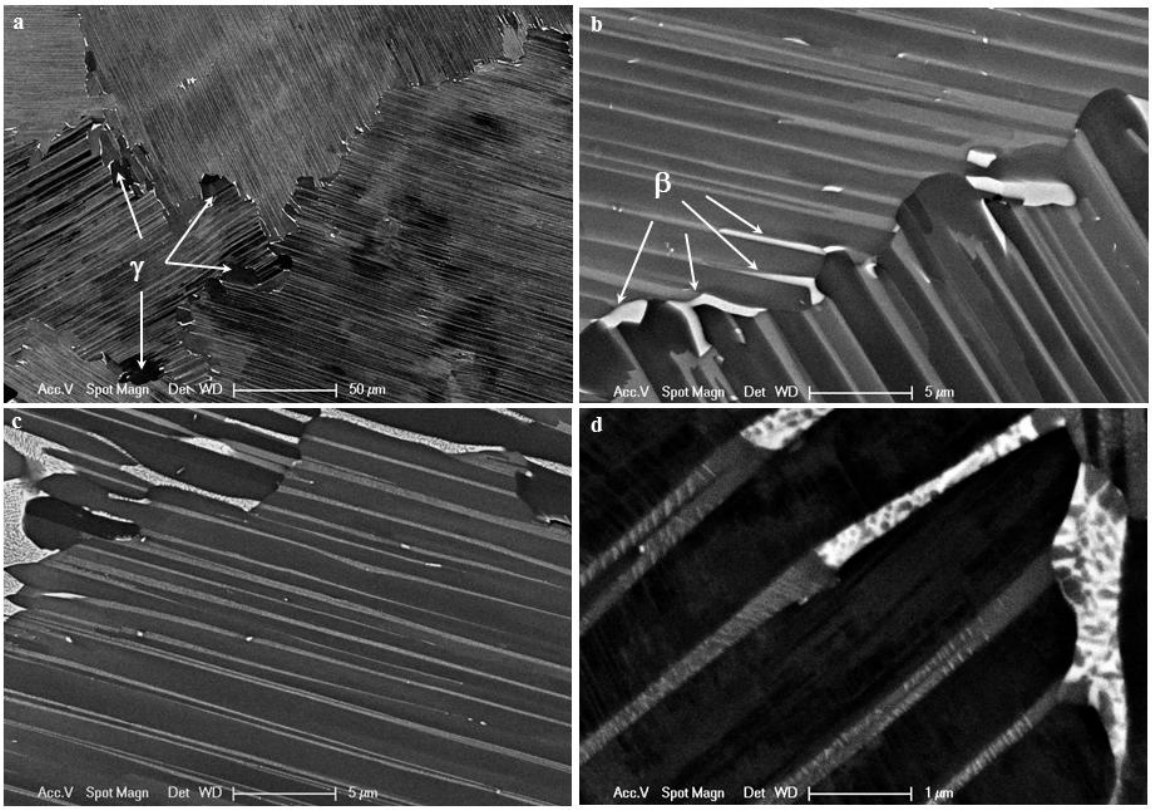

Fig. 1 SEM BSE images showing the lamellar microstructure of alloy Ti-46Al-5Nb-1W (a, b) before and (c, d) after 10000 h exposure at 700°C.

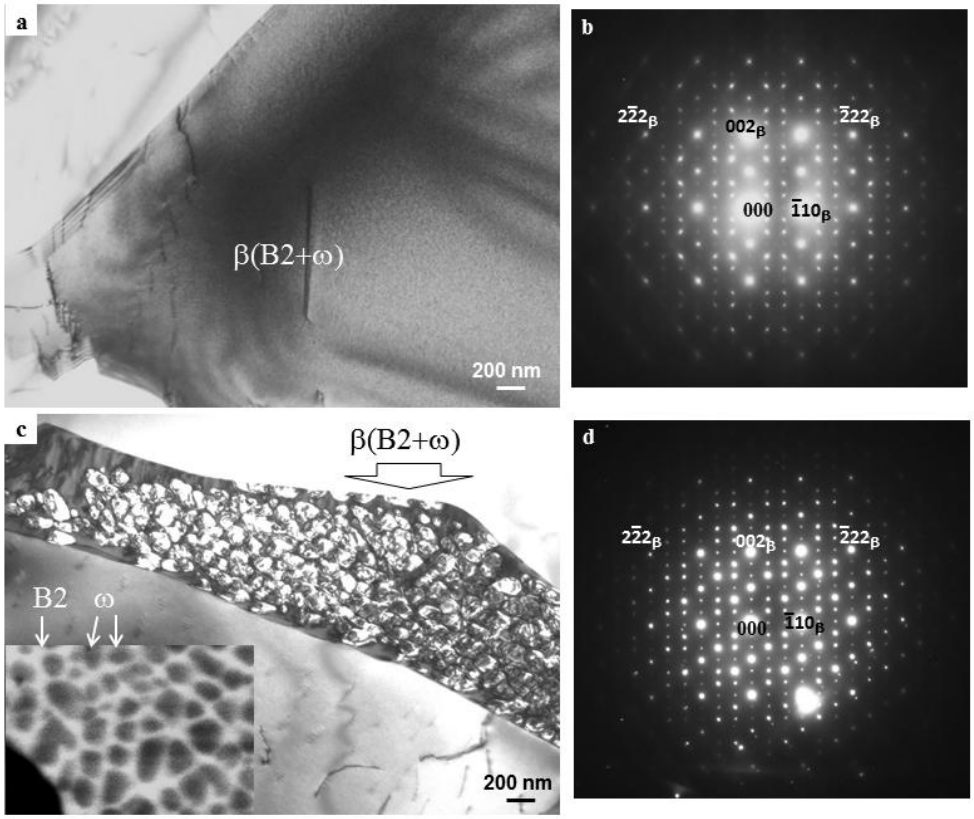

Fig. 2 TEM images shown ω particles in a B2 grain of alloy Ti-46Al-5Nb-1W, (a) BF image at 0h and (c) CDF image after10000 h exposure at 700°C. (b) and (d) Corresponding diffraction pattern taken from β(B2+ω) grain in (a) and (c), respectively.

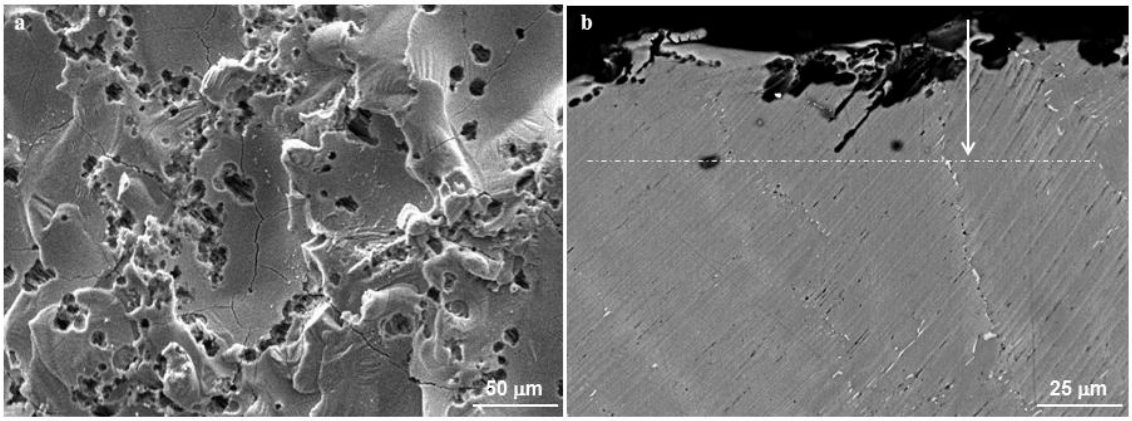

Fig. 3 SEM images showing (a) the normal (SE) and (b) cross sectional view (BSE) of the EDM surface before exposure (crack ~50µm).

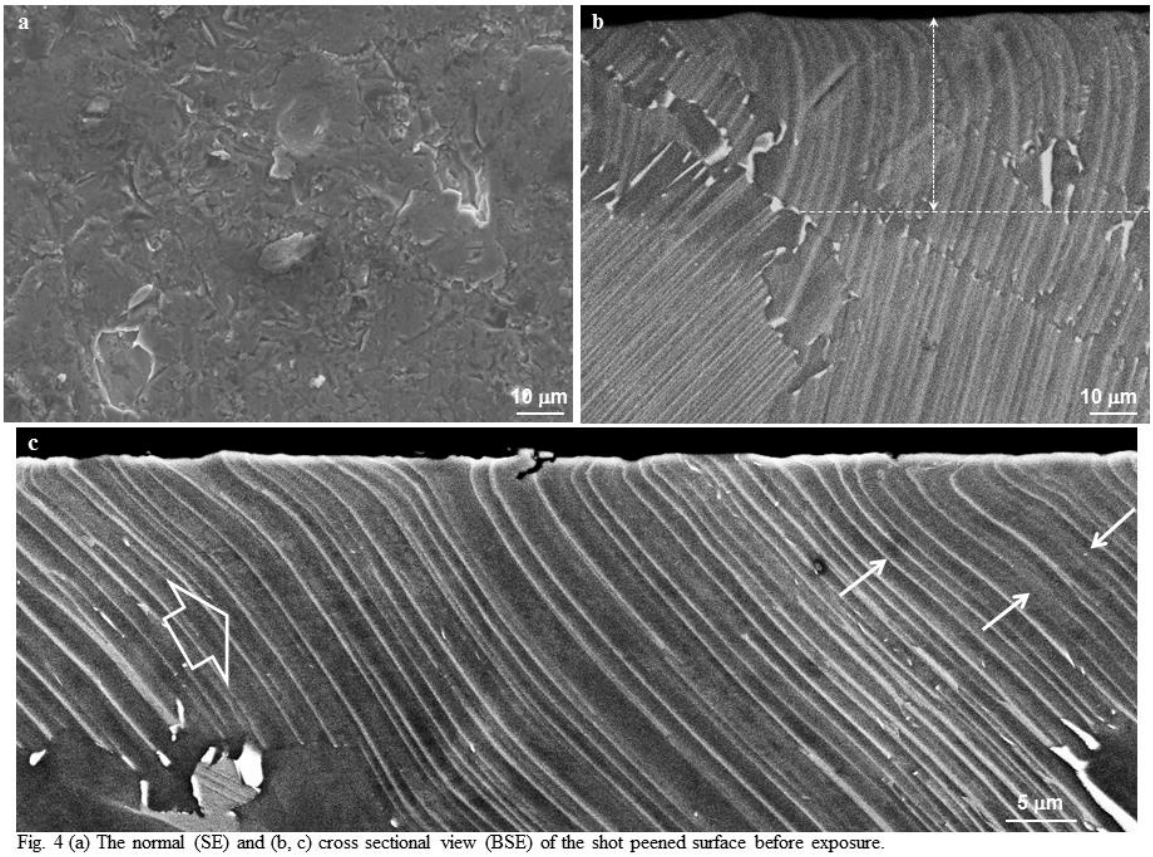

Fig. 4 (a) The normal (SE) and (b, c) cross sectional view (BSE) of the shot peened surface before exposure.

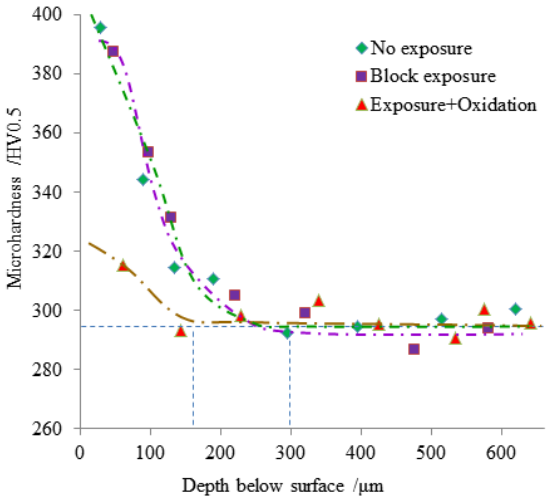

Fig. 5 Micro hardness profiles of shot peened specimens before and after thermal exposure.

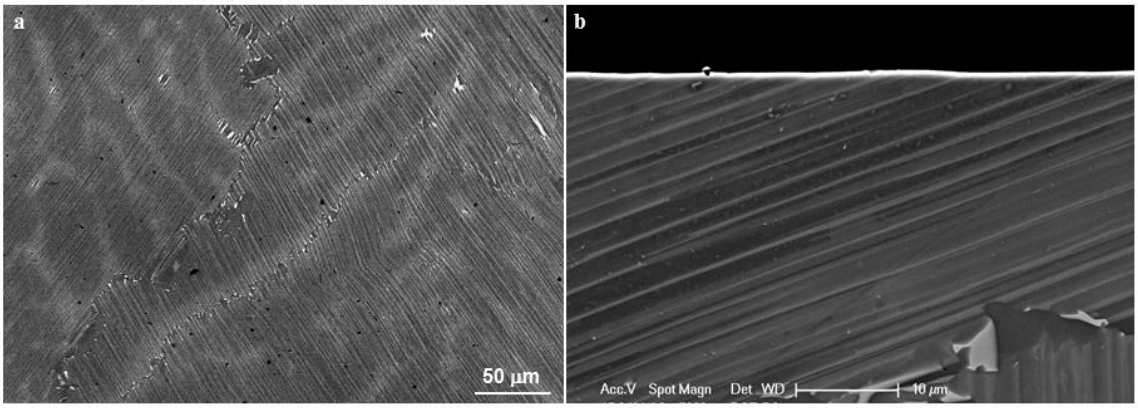

Fig. 6 (a) The normal (BSE) and (b) cross sectional view (SE) of the electropolished surface before exposure, which is smooth and nearly defect-free.

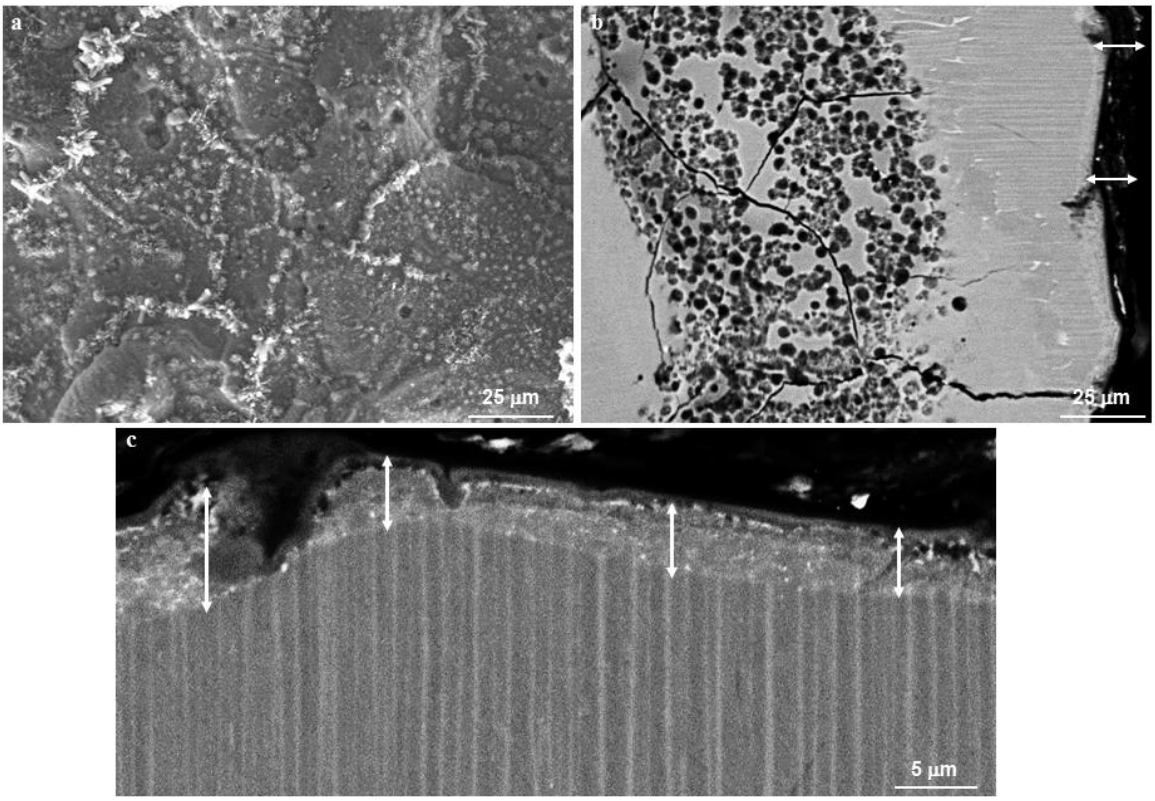

Fig. 7 (a) The normal view (SE), and (b), (c) cross sectional view (BSE images) of the EDM surface after individual exposure-oxidation at 700°C for 10000 h. Note that the oxidation scale is ~ 15 μm thick (b), followed by an α_2-free layer, ~ 5 μm thick (c). Also noted is a subsurface oxidation characterised by numerous oxidation pits and microcraks in (b).

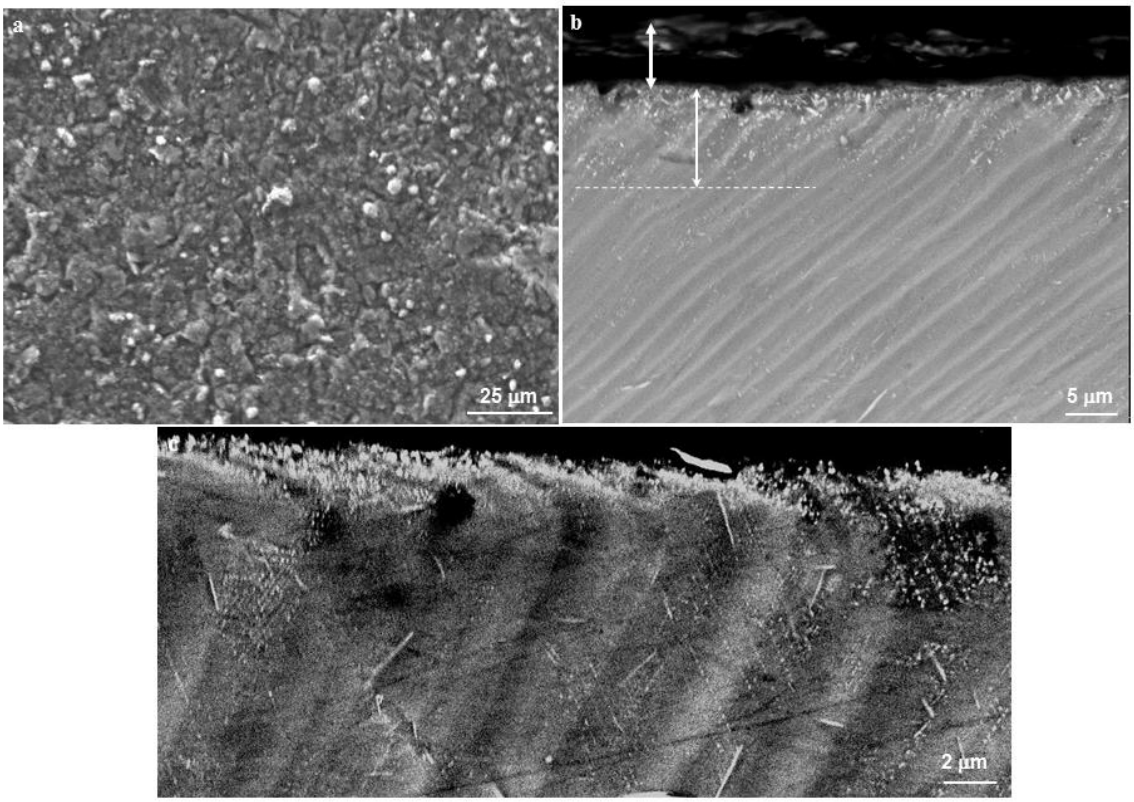

Fig. 8 (a) The normal view (SE), and (b), (c) cross sectional view (BSE) of the shot peened surface after exposure-oxidation at 700°C for 10000 h. Note that the oxidation scale is ~ 5 µm thick, followed by a subsurface region (~ 10 µm thick) covered by a high density of white particles (b).

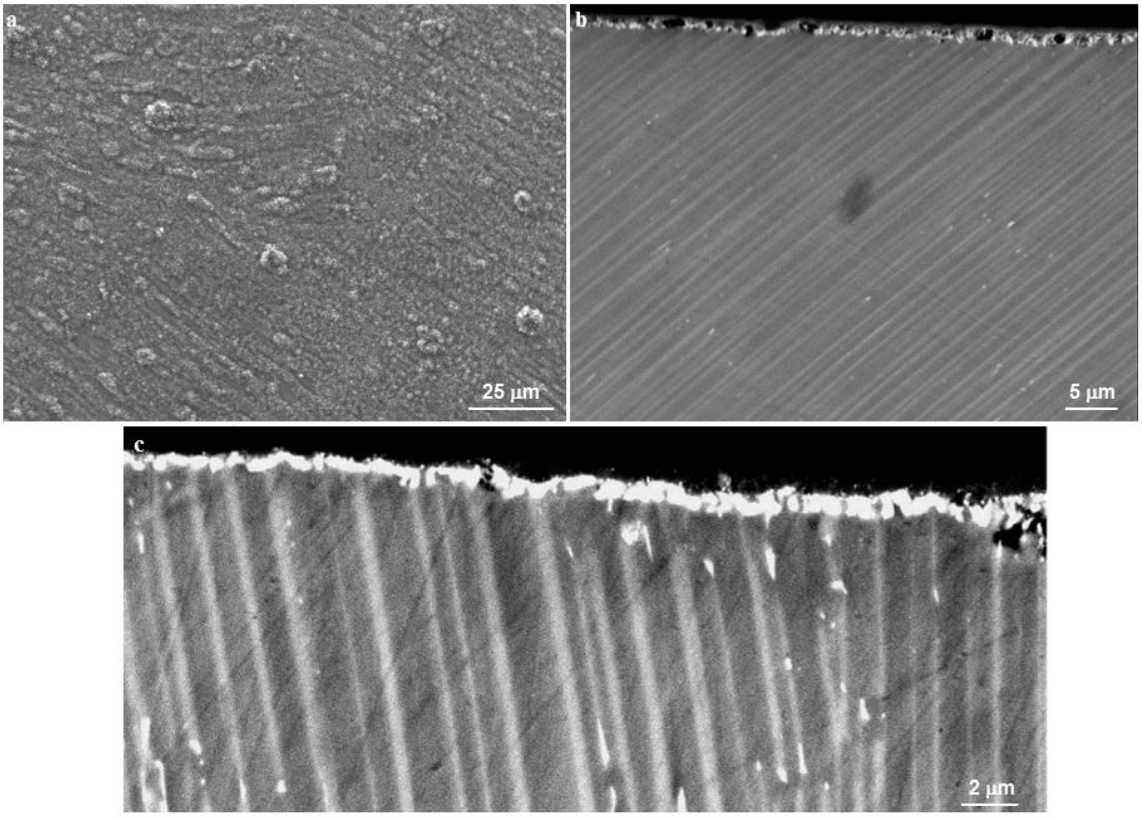

Fig. 9 (a) The normal view (SE) and (b), (c) cross sectional view (BSE) of the electropolished surface after exposure-oxidation at 700°C for 10000 h. Note that the oxidation scale is very thin, followed by a semi-continuous layer consisting of white particles.

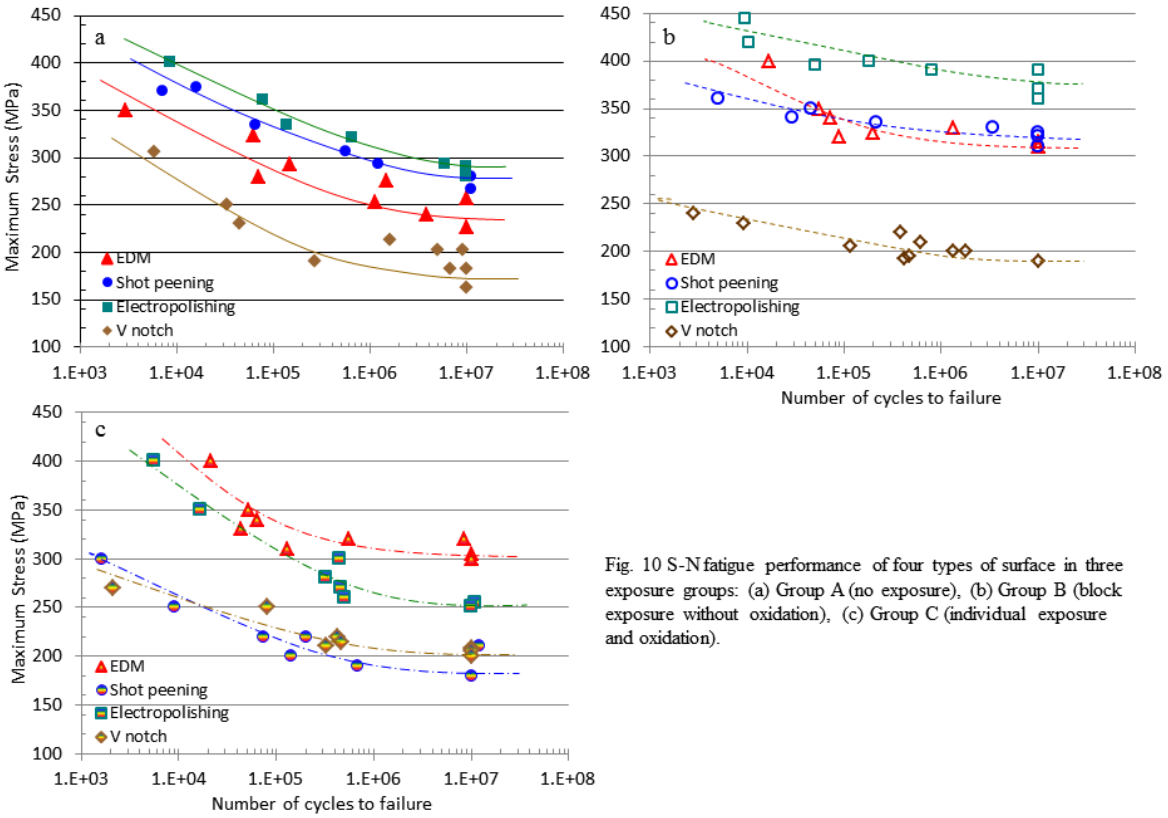

Fig. 10 S-N fatigue performance of four types of surface in three exposure groups: (a) Group A (no exposure), (b) Group B (block exposure without oxidation), (c) Group C (individual exposure and oxidation).

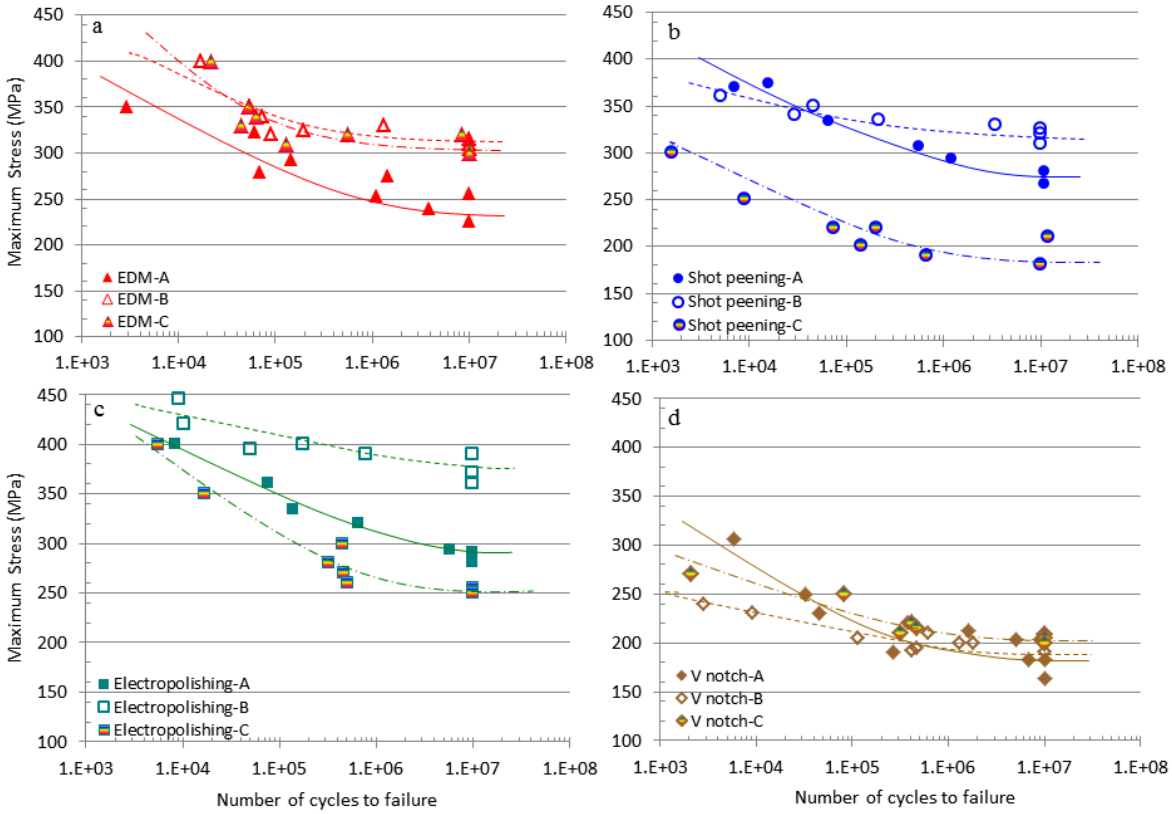

Fig. 11 S-N fatigue performance of four types of surface in three exposure conditions: (a) EDM, (b) shot peening, (c) electropolishing and (d) V notch (A, B, C denote Group A, B, and C, respectively).

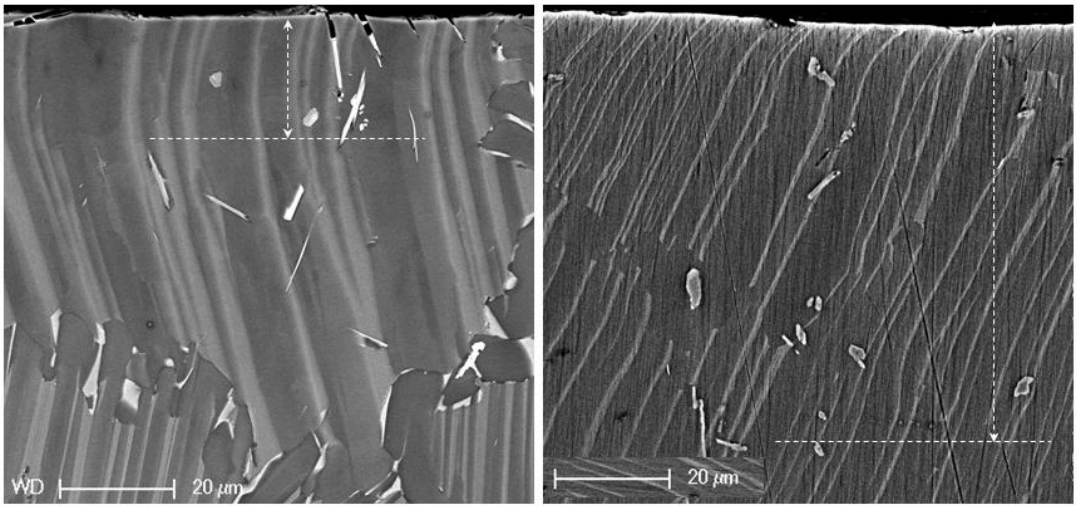

Fig. 12 BSE images showing cross sectional view of the deformed surface layer produced by the same shot peeing process, (a) alloy Ti-44Al-5Nb-1W-1B and (b) alloy Ti-45Al-2Mn-2Nb-0.8vol%TiB2.

Highlights

- Study on fatigue response of designed surfaces and microstructure for a TiAl alloy
- Phase transformation and microstructure change are induced by thermal exposure
- Ti-46Al-5Nb-1W under fatigue is sensitive to surface damage but not to V-notch
- Shot peening and electropolishing offer a moderate increase in fatigue strength
- Both beneficial and detrimental effects on fatigue are induced by thermal exposure